Anomalously Supercooled H_2-D_2 Mixtures Flowing inside a Carbon Nano Tube†

I-Ya Chang[a], Shutaro Yamaoka[a] and Kim Hyeon-Deuk*[a]

Abstract H_2 and D_2 molecules condensed in a carbon nano tube (CNT) and their nonequilibrium flow through the nano pore offers a key test to reveal mass molecular transport and separation of the purely isotopic molecules that possess the same electronic potential but the twice different mass inducing differently pronounced nuclear quantum effects (NQEs) such as nuclear delocalization and zero-point energy. Taking advantage of the non-empirical quantum molecular dynamics method developed for condensed H_2-D_2 molecules that can describe various kinds of condensed phases and thermodynamic states including uneven density and a shear flow, we investigated the condensed isotopic H_2-D_2 mixtures flowing inside the nanoscale adsorbable CNT. We found that, in any mixtures, the more delocalized H_2 molecules are more supercooled than the less delocalized D_2 molecules in a two-dimensional liquid film adsorbed around the CNT well, and that the stronger supercooling of the H_2 molecules than the D_2 molecules in an equilibrium state becomes more enhanced under the nonequilibrium flow due to the isotope-dependent flow-induced condensation, demonstrating the anomalous condensed-phase quantum sieving under the nonequilibrium flow and its dependence on the mixing ratio and temperature. The differently pronounced NQEs of the purely isotopic molecules essentially influence the condensed adsorption and their flows occurring in the nanoscale CNT, which should be distinguished from a dilute gas adsorption. The predicted properties and obtained physical insights in this paper will help in experimentally controlling condensed H_2-D_2 mixtures, and open a new strategy and innovative design of nanoporous materials for adsorptive separation of condensed-phase mixtures under a nonequilibrium flow not of a dilute gas mixture in an equilibrium state.

1 Introduction

H_2 and D_2 are purely isotope molecules possessing the same electronic potential but the twice different mass inducing differently enhanced nuclear quantum effects (NQEs) such as nuclear delocalization and zero-point energy and different thermodynamic properties.[1–7] Path integral molecular dynamics methods (i-PI) implemented in the CP2K program package to include the quantum mechanical nature of atomic nuclei have been intensively developed to evaluate equilibrium properties of molecules like CH_4, CH_5^+ and H_2O, which should be applicable to hydrogen and deuterium molecules.[8,9] Mixtures of the H_2 and D_2 molecules thus have been an ideal and attractive binary liquid, and the separation of H_2 and D_2 molecules is of great importance for numerous applications.[10] The current separation processes of hydrogen isotopes require a high cost and energy due to the complex operation procedures and low separation efficiency. Establishing a convenient and inexpensive process to effectively separate D_2 molecules from H_2 molecules has been a practical issue over the past few years.

Adsorptive separation using nanoporous materials can be a simple and efficient solution.[10–13] In fact, various porous materials like carbon nano tubes (CNTs)[14] and metal-organic frameworks[10,15–17] have been examined for the effective hydrogen isotope separation. The main key has been a development of a suitable adsorbent for high selectivities for gaseous isotope H_2-D_2 mixtures by the quantum sieving exploiting their different thermal de Broglie wavelength.[10–22]

In addition to such gas adsorption essentially determined by an interaction potential between a single molecule and a porous surface, condensed molecules confined in a nano pore and their nonequilibrium flow inside the nano pore offers a challenging system for revealing mass molecular transport and separation.[23–30] Actually, creation of a condensed molecular flow through a CNT that provides a selective transport including adsorption/desorption and an extraordinarily fast flux has a wide range of industrial and scientific applications such as energy transfer and storage as well as molecular sensing and separation.[25–28] The NQEs should play a critical role in correctly describing such nonequilibrium flow of the condensed H_2 and D_2 molecules inside a CNT where temperature and density change in a single nanometer range.[23]

The nuclear and electron wave packet molecular dynamics (NEWPMD) method has successfully reproduced the various experimental observations without any empirical parameter and model potential: *e*.g. (1) the structures, transport coefficients, and intramolecular vibrational frequency in the H_2 liquids,[31–33] (2) the periodic lattice structure stably formed below the freezing temperature, vibrational amplitude and collective phonon frequency in the H_2 solids,[34] (3) the single cm^{-1}-order jump of the H-H vibrational frequency through

[a]*Department of Chemistry, Kyoto University, Kyoto 606-8502, Japan. Fax: +81-75-753-4000; Tel: +81-75-753-4021; E-mail: kim@kuchem.kyoto-u.ac.jp*

† Electronic Supplementary Information (ESI) available: Additional structural and dynamical information on hydrogen and deuterium molecules.

the liquid-solid phase transition[34], (4) the thermal conductivity of the H_2 liquid achieving a temperature gradient[35], (5) the D-D bond length and diffusion coefficient of the D_2 liquid[36], and (6) the slowdown of the translational dynamics of the H_2-D_2 mixture at the optimal mixing rate[37]. The above reproduction of the experimental results in the far-different phases and thermodynamic states demonstrated that the NEWPMD method successfully describes the different thermal de Broglie wavelength of the H_2 and D_2 molecules and the real thermodynamic states at the same temperature and densities as the experimental values.

In this paper, taking advantage of the NEWPMD method, we investigate nonequilibrium flows of condensed H_2-D_2 mixtures exhibiting the strong and differently pronounced NQEs inside a nanoscale adsorbable CNT, demonstrating the anomalous condensed-phase quantum sieving and its dependence on the mixing ratio and temperature. Various kinds of complex condensed phases and thermodynamic states including uneven density and a shear flow can dynamically appear and disappear in the nonequilibrium condensed flows inside the adsorbable CNT, which cannot be revealed by a simple analysis of the interaction potential energy between a single molecule and the CNT surface nor by a path integral method requiring an equilibrium partition function with uniform temperature and density.[23,35]

2 Methods

The NEWPMD method describes floating and thawed Gaussian nuclear wave packets (NWPs) via the time-dependent Hartree method, and electron wave packets (EWPs) through the perfect-pairing valence bond theory that treats the Pauli exclusion energy.[31,32] Because the NEWPMD method is based on the following microcanonical equations of motion (EOMs) to time-evolve NWPs derived through the time-dependent quantum variational principle[31–39],

$$\dot{\mathbf{P}}_K(t) = -\frac{\partial H_{\rm ext}}{\partial \mathbf{R}_K(t)} + \mathbf{F}_{CNT}, \tag{1}$$

$$\dot{\mathbf{R}}_K(t) = \frac{\partial H_{\rm ext}}{\partial \mathbf{P}_K(t)}, \tag{2}$$

$$\dot{\Pi}_K(t) = -\frac{1}{3}\frac{\partial H_{\rm ext}}{\partial \Omega_K(t)}, \tag{3}$$

and

$$\dot{\Omega}_K(t) = \frac{1}{3}\frac{\partial H_{\rm ext}}{\partial \Pi_K(t)}, \tag{4}$$

the NEWPMD method can simulate real-time dynamics of hydrogen and deuterium molecules even under a nonequilibrium and non-uniform flow. Real-time dynamics of the NWPs is specified uniquely by the four time-dependent variables: The three-dimensional Kth nuclear coordinate $\mathbf{R}_K(t)$ and the Kth NWP width $\Omega_K(t)$ as well as their conjugate momenta $\mathbf{P}_K(t)$ and $\Pi_K(t)$, respectively. The non-empirical extended Hamiltonian $H_{\rm ext} = H_{\rm ext}(\{\mathbf{P}_K(t)\},\{\mathbf{R}_K(t)\},\{\Pi_K(t)\},\{\Omega_K(t)\})$, a sum of the kinetic energy of nuclei and electrons, and the three electrostatic interaction energy of electron-electron, nucleus-nucleus and nucleus-electron, was explicitly derived by treating each of nucleus and electron as a thawed Gaussian wave packet.[31,32,39] The NEWPMD approach can reproduce a long-range dispersion force that a conventional density functional theory (DFT) cannot provide.[39,40] It should be noted that the EWPs adjust their positions and width to the NWP's of the same molecule at each moment of actual time evolution.[31–39] The simple EOMs (1)-(4) guarantee stable and long-time molecular dynamics simulations of condensed H_2 and D_2 molecules. The only difference between H_2 and D_2 molecules is the atomic mass, 1.00794 for H and 2.01410 for D, respectively; the EWP part of the NEWPMD program is exactly the same regardless of the isotopes.

In this paper, we calculated real-time microscopic dynamics of H_2 and D_2 molecules flowing inside a single wall CNT, CNT(15,0), at high and low temperatures.(Figs.S1-S2, ESI†) CNT(15,0) whose radius is 5.87167 Å was placed in the periodic unit cubic cell matching its axis to the z-axis of the periodic unit cell. The molecule-CNT(15,0) interaction force $\mathbf{F}_{CNT}$ in eq.(1) was determined by the DFT computations with the PBE-D2 scheme[41] and PAW pseudopotentials using the VASP package[42].(See the computational details in Section S1 and Figs.S3-S4, ESI†)

The effective molar volume was calculated as $25.55 \times 10^{-6}\mathrm{m}^3/\mathrm{mol}$ excluding the region where any molecule cannot reach due to the extremely high interaction potential energy between the molecule and CNT(15,0).[43] It is close to the vapor-pressure molar volume for D_2 around 25 K, $25.17 \times 10^{-6}\mathrm{m}^3/\mathrm{mol}$, and thus smaller than the vapor-pressure molar volume for H_2 around the same temperature, $31.28 \times 10^{-6}\mathrm{m}^3/\mathrm{mol}$.[1] The five mixing ratios were set as the D_2 ratios of 0 %, 25 %, 50 %, 75 %, and 100 % which we will call in this paper the 1:0 mixture, 3:1 mixture, 1:1 mixture, 1:3 mixture, and 0:1 mixture, respectively. We performed cooling and equilibration runs by the velocity scaling thermostat for 5 ps and then by the stochastic thermostat for several hundreds picoseconds at the aimed temperatures, respectively.[31,32] After reaching the equilibration, we carried out the equilibrium NVE (microcanonical) simulations for 3 ns. Integration of the EOMs (1)-(4) were performed by the velocity-Verlet method with the time step 0.1 fs for the cooling and equilibration runs and with 0.25 fs for the NVE (microcanonical) simulations. In order to achieve a nonequilibrium molecular flow inside CNT(15,0), the z-component of the center of mass (COM) velocity of a

molecule, V_z, was reversed every 25 fs if its value is negative and if the molecule exists within the furthest one-fiftieth region of the unit cell along the z-axis.[23,43] Each nonequilibrium simulation performed by the velocity-Verlet method with the time step 0.1 fs includes a relaxation process during an initial few nanoseconds that corresponds to a transition from an initial equilibrium state to a steady-state nonequilibrium state. After the steady-state nonequilibrium flows were attained, we again performed the NVE (microcanonical) simulations of 3 ns by the velocity-Verlet method with the time step 0.25 fs.(Figs.S5-S6, ESI†))

3 Results and discussions

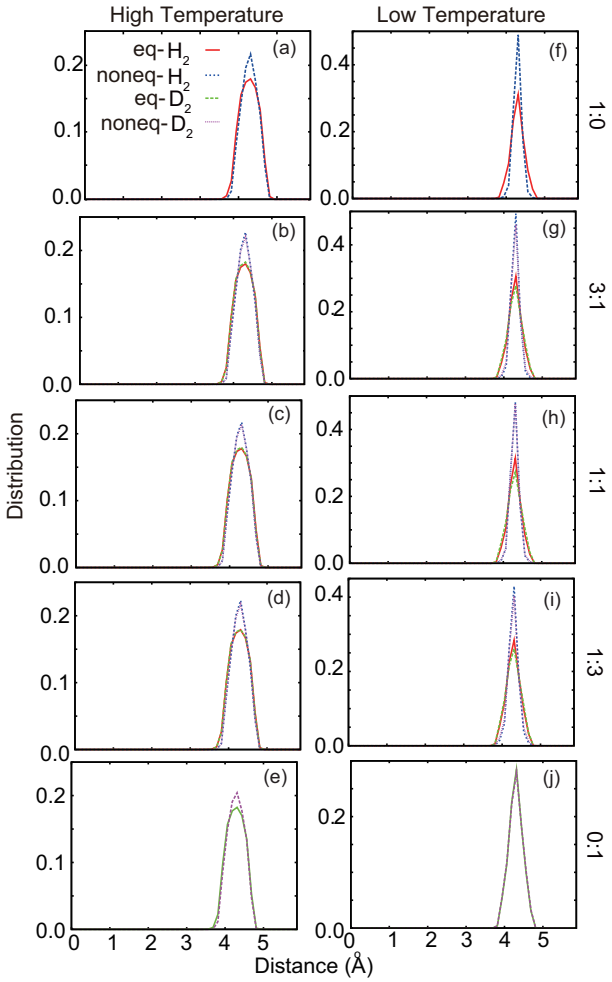

Fig. 1 Radial distributions of H_2 and D_2 molecules as a function of the radial distance from the CNT(15,0) center in the equilibrium and nonequilibrium states at (a-e) the high temperature and (f-j) the low temperature.

3.1 Radial distributions

All the H_2 and D_2 molecules are adsorbed and trapped around the CNT(15,0) well with the current temperatures regardless of the mixing ratios. (Fig.1) The H_2 and D_2 molecules are thus condensed into a two-dimensional (2D) liquid film around the CNT(15,0) well, which should be distinguished from a dilute gas adsorption where no molecular condensation exists and intermolecular interaction is almost absent. There is little difference between the condensed H_2 and D_2 adsorption at the high temperature although their vapor-pressure molar volume is clearly different.[1,37](Fig.1(a-e)) The molecular condensation around the CNT(15,0) well is more enhanced under the nonequilibrium flow regardless of the mixing ratio as the higher peaks of the nonequilibrium molecular distributions show. The excess heat caused by the enhanced adsorption contributes to the higher temperature in the nonequilibrium states than in the equilibrium state.(Figs.S1-S2, ESI†) This enhancement can be called the flow-induced condensed adsorption that cannot be explained by a simple increase of the temperature and inner pressure since the increase of the temperature and inner pressure rather expands the region where molecules can exist[37], and that should be distinguished from the single-file rapid transport of water molecules along a nano tube[24,25,44–49] because the present molecules still can diffuse in the 2D cylindrical region around the CNT(15,0) well. The flow-induced condensation occurs because the molecules are compressed along the CNT axis by the increased pressure due to the nonequilibrium flow along the z-axis and the more molecules concentrate into the CNT well region where some space is induced by the compression, making the molecular flow narrower.

The lower temperature induces sharper molecular distributions both in the equilibrium and nonequilibrium states, meaning that the 2D liquid films become thinner and denser around the CNT well.(Fig.1(f-j)) The molecular condensation under the nonequilibrium flow is more apparent at the low temperature than at the high temperature. Especially at the low temperature, the H_2 molecules tend to be more condensed than the D_2 molecules reflecting that the H_2 molecules are more supercooled compared to the D_2 molecules(Fig.1(g-i)); the present effective molar volume is more cramped for the more delocalized H_2 molecules than for the less delocalized D_2 molecules, which stems from the differently enhanced NQEs of the purely isotopic molecules possessing the same EWPs but the twofold mass; the longer bond and larger NWP width of the H_2 molecule make the H_2 molecule more delocalized than the D_2 molecule. In fact, the radial distributions become sharper as the D_2 mixing ratio decreases–the different NQEs of the isotope mixtures play a role for the condensed adsorption of the 2D liquid films.

It is also remarkable that the flow-induced ordering is in-

efficient for the D_2 molecules; the difference between the equilibrium and nonequilibrium radial distributions becomes smaller as the the D_2 ratio increases.(Figs.1(e) and 1(j)) The equilibrium and nonequilibrium distributions are almost overlapped in Fig.1(j), and, actually, there seems little difference between the snapshots drawn in Fig.S7(j) and Fig.S8(j)(ESI†) compared to the other four mixtures drawn in Fig.S7(f-i) and Fig.S8(f-i)(ESI†). The less delocalized D_2 molecules are less condensed by the nonequilibrium flow because the less delocalized D_2 molecules are originally not dense nor supercooled and do not easily become condensed since the current molar volume was set close to the D_2 vapor-pressure molar volume around 25 K. The lower flow velocity with the higher D_2 mixing ratio also contributes to the less-effective condensation.(See Figs.S9-S10, ESI†)

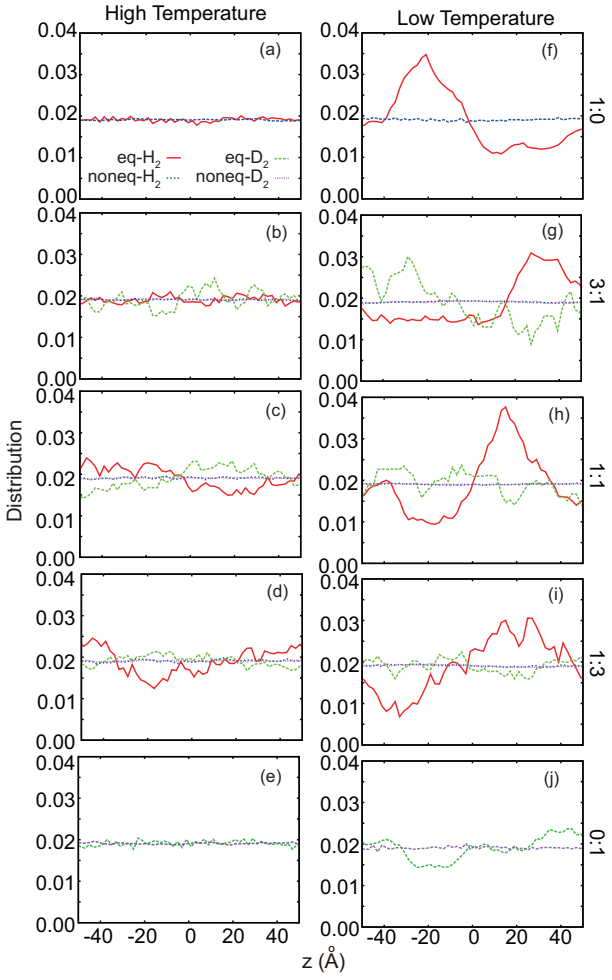

Fig. 2 Axial distributions of the H_2 and D_2 molecules along the CNT axis (z-axis) in the equilibrium and nonequilibrium states at (a-e) the high temperature and (f-j) the low temperature.

3.2 Axial distributions

The axial distributions along the z-axis characterize the 2D mixture films more clearly.(Fig.2) Although most of the axial distributions are flat at the high temperature, the distributions of the H_2 molecules are more structured in the 1:1 and 1:3 mixtures (Figs.2(c) and 2(d)); a small number of the H_2 molecules tend to aggregate rather than being uniformly dispersed, which is essentially different from an isolated dilute gas adsorption.

At the lower temperature, the axial distributions of the H_2 molecules become anomalously structured due to the strong supercooling of the 2D mixture films. As can be seen in Figs.2(f-i), the stronger hydrogen NQEs make the axial distributions of the more delocalized H_2 molecules drastically structured compared to the distributions of the less delocalized D_2 molecules. Since degrees of freedom for the molecules to diffuse are quite limited inside the 2D mixture films, the isotope-dependent uneven structures can survive for an extremely long time.

In Fig.2, all the axial distributions are flat in the nonequilibrium states owing to the steady-state flow. However, as Fig.S8(ESI†) demonstrates, the 2D liquid films are anomalously structured and extremely non-uniform under the nonequilibrium flow. The 2D mixtures are almost separated into the condensed and vacuum regions at the low temperature except for the 0:1 mixture. This should be called the flow-induced inhomogeneity occurring in the 2D mixture films.

3.3 Time correlation functions of the center of mass velocity

Molecular dynamics appearing in CNT(15,0) can be discussed through time correlation functions (TCFs) of the COM molecular velocity $\mathbf{V}(t)$.(Fig.3 and Fig.S11, ESI†) The $\mathbf{V}$-TCFs are defined as $\langle V_i(t)V_i(0)\rangle/\langle V_i^2(0)\rangle$ with $i = x$, y, and z where $\langle\cdots\rangle$ means an ensemble average over different initial times and molecules. The $\mathbf{V}$-TCF oscillates faster for the lighter H_2 molecules than for the heavier D_2 molecules.

The oscillation of the V_x-TCF and V_y-TCF directly links to the vibrational dynamics of adsorbed molecules around the CNT well; actually, such oscillating behavior does not appear in simple bulk systems[36,37]. The V_x-TCF and V_y-TCF are almost identical because of the geometric symmetry, guaranteeing the uniformity of the 2D mixture films along the azimuthal angle on the xy-plane.(Figs.3(a) and 3(b), and Figs.3(d) and 3(e)) All the mixtures exhibit the almost similar V_x-TCF and V_y-TCF for the same isotope regardless of the mixing ratio since the short-time TCFs are determined by the local vibrational dynamics around the CNT well without a long-range diffusion. The oscillation of the V_x-TCF and V_y-TCF is more significant at the low temperature due to the more condensed liquid structure caused by the stronger supercooling.

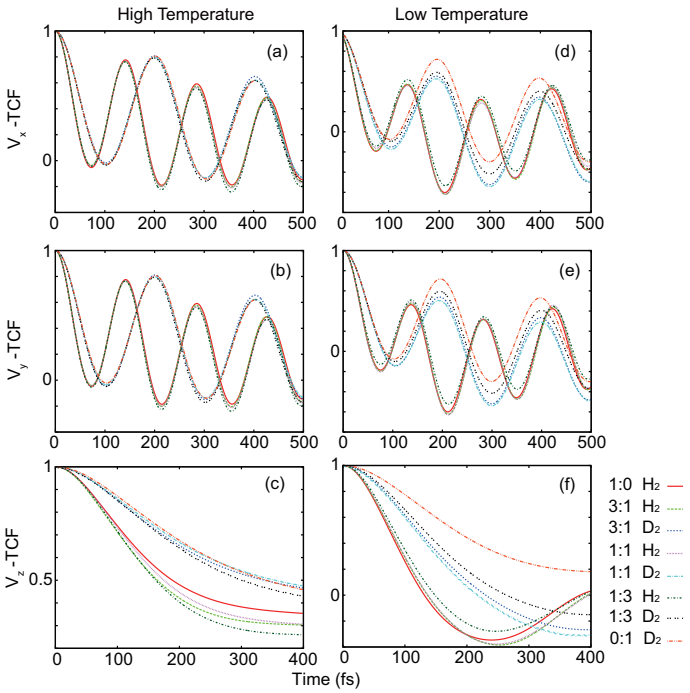

Fig. 3 TCFs of the COM molecular velocity $\mathbf{V}(t) = (V_x, V_y, V_z)$ under the nonequilibrium flows at (a-c) the high temperature and (d-f) the low temperature.

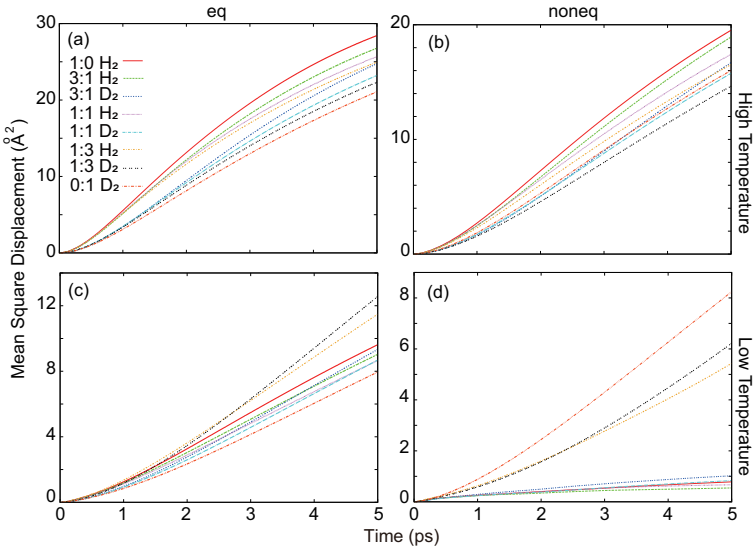

Fig. 4 MSDs of the H_2 and D_2 molecules on the CNT(15,0) cross-section (the *xy*-plane) at (a) the high temperature in the equilibrium states, (b) the high temperature under the nonequilibrium flows, (c) the low temperature in the equilibrium states, and (d) the low temperature under the nonequilibrium flows.

The short-time oscillation disappears in the V_z-TCF since it expresses molecular dynamics along the z-axis which is not related to the local vibrational dynamics around the CNT well.(Figs.3(c) and 3(f)) Instead, the V_z-TCF oscillates slowly reflecting the slow deformation and long-time diffusive dynamics along the z-axis. The smoother deformation and diffusion at the high temperature in the equilibrium state even leads to the monotonic decay of the V_z-TCF without oscillation.(Fig.S11(c), ESI†) The flow-induced condensed adsorption totally makes the oscillational behaviors of the **V**-TCFs more apparent in the nonequilibrium state than in the equilibrium state.(Compare Fig.3 and Fig.S11, ESI†)

3.4 Mean-square-displacements

Mean-square-displacements (MSDs) on the CNT(15,0) cross-section (the *xy*-plane) characterize kinetic and diffusive dynamics taking place in the 2D mixture films.(Fig.4 and Fig.S12, ESI†) Since the initial MSDs reflect a short-time kinetic motion, the initial MSDs of the lighter H_2 molecules increase faster than the initial MSDs of the heavier D_2 molecules regardless of the temperature.(Figs.4(a), 4(b), and S12) At the high temperature, the gradients of the MSDs of the lighter H_2 molecules and the heavier D_2 molecules become closer for the same mixture as time proceeds. This is because the gradients of the long-time MSDs are determined by the long-range diffusion involving enough energy exchange among the H_2 and D_2 molecules. For example, as shown in Figs.4(a) and 4(b), the MSD gradient of the heavier D_2 molecules in the 3:1 mixture is larger than the MSD gradient of the lighter H_2 molecules in the 1:3 mixture around 5 ps. The deceleration of the MSDs in the long-time region originates from the restricted diffusion dynamics occurring in the confined 2D mixture films. The nonequilibrium MSDs are totally smaller than the equilibrium MSDs in any mixtures; the condensed adsorption enhanced by the nonequilibrium flow suppresses the diffusion. It should be noted that, because the flow-induced condensation is less enhanced with increasing the D_2 mixing ratio (Fig.1(e)), the suppression of the nonequilibrium MSD of the 0:1 mixture is smaller, resulting in the larger MSD of the heavier 0:1 mixture than the lighter 1:3 mixture in Fig.4(b).

The extreme supercooling dominates the long-time MSDs especially at the low temperature. (Figs.4(c) and 4(d)) The MSDs of the lighter H_2 molecules and the heavier D_2 molecules do not match even in the same mixture due to the poor energy exchange among the H_2 and D_2 molecules at the low temperature. In the equilibrium state, the 1:3 mixture exhibits the fastest diffusion. This fastest diffusion stems from the diffusive dynamics determined by the balance of the liquid mass and the extent of the supercooling[37]: On one hand, the lighter mixture exhibits the faster diffusion and *vice versa*. On the other hand, the supercooling mainly caused by the H_2

molecules decelerates the diffusion dynamics due to the structured and non-uniform mixture solvation. The fastest diffusion appearing in the 1:3 mixture is also evidenced by the flattest axial distribution of the majority component (the D_2 molecules in the 1:3 mixture) shown in Fig.2(i). Also, in the same mixture, the MSD of the heavier D_2 molecules exceeds the MSD of the lighter H_2 molecules at the low temperature as time goes by. Such anomalous mobility order of the H_2 and D_2 molecules demonstrates the significant supercooling of the H_2 molecules, and agrees with the previously observed anomalous diffusion order and selectivity of H_2 and D_2 molecules.[50]

The MSDs are more suppressed under the nonequilibrium flow at the low temperature than at the high temperature, which stems from the flow-induced condensation more enhanced at the low temperature.(See Figs.1(f-i)) The more significantly supercooled H_2 molecules in the equilibrium state become even more supercooled under the nonequilibrium flow. Actually, in the 0:1 mixture whose flow-induced condensation is negligible as shown in Fig.1(j), the MSDs are almost similar in the equilibrium and nonequilibrium states, resulting in the largest MSD of the 0:1 mixture under the nonequilibrium flow.(See Figs.4(c) and 4(d)) The originally more supercooled the mixture is in the equilibrium state, the more supercooled the mixture becomes in the nonequilibrium state due to the isotope-dependent flow-induced condensation. The above insights for the anomalous diffusive dynamics appearing in the 2D mixture films could not be obtained only by a single molecule-surface potential calculation.

We note that the H_2-D_2 mixtures in CNT(15,0) are in the supercooled liquid state. If the H_2-D_2 mixtures were solid-like, their MSDs as a function of time would be completely flat reflecting a solid phonon mode.[34] However, the current MSDs of the H_2-D_2 mixtures on the xy-plane monotonically increases even at the low temperature under the flow (Fig.S12(c)), clearly indicating that the present H_2-D_2 mixtures are in the supercooled liquid state. Because the current mixtures form a 2D film liquid, their radial distribution functions (RDFs) are different from a RDF of normal hydrogen liquids[31], making the judgement of a supercooled liquid or a solid quite difficult.(Fig.S13, ESI†) The almost uniform distributions of the molecular orientation $\phi(t)$ from the z-axis shown in Fig.S14 (ESI†) rather clearly demonstrate that the H_2-D_2 mixtures in CNT(15,0) is not solid-like; if the H_2-D_2 mixture were solid-like, the distributions of the molecular orientation $\phi(t)$ would have clear peaks[34].

3.5 Power spectra of the molecular orientation

The effect of the isotope-dependent flow-induced condensation can be further seen in molecular orientational dynamics (Figs.5) rather than in the almost uniform orientational distributions (Fig.S14). The power spectra of the molecular orientation $\phi(t)$ do not show any clear peak at the high temperature, indicating that a clear librational motion does not exist in the 2D mixture films at the high temperature.(Figs.5(a) and 5(b)) In contrast, the $\phi(t)$-power spectra of H_2 components at the low temperature have a clear shoulder even in the equilibrium states, demonstrating that H_2 molecules are more supercooled and structured than the D_2 molecules at the similar temperature and density.(Fig.5(c)) The clear librational motions appear at the low temperature under the nonequilibrium flows as evidenced by the 100 cm^{-1}-order low-frequency peaks reflecting the strong supercooling.(Fig.5(d)) The stiff solvation structures caused by the strong condensation at the low temperature lead to the formation of the librational potentials. The smaller moment of inertia of the H_2 molecules provides the higher librational peak frequency than the larger moment of inertia of the D_2 molecules. Because the flow-induced condensation is almost absent in the 0:1 mixture at the low temperature, the $\phi(t)$-power spectrum of the 0:1 mixture does not significantly differ in the equilibrium and nonequilibrium states.

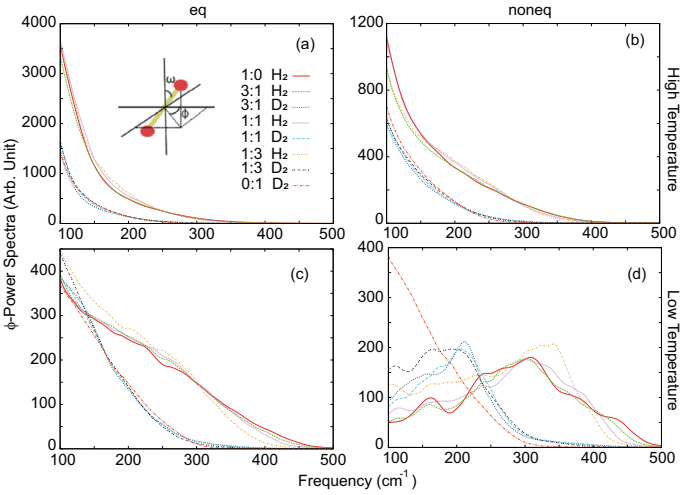

Fig. 5 Power spectra of the molecular orientation $\phi(t)$ from the z-axis at (a) the high temperature in the equilibrium states, (b) the high temperature under the nonequilibrium flows, (c) the low temperature in the equilibrium states, and (d) the low temperature under the nonequilibrium flows.

3.6 Intramolecular structures

Finally, we show the mixing ratio as well as the macroscopic nonequilibrium flow can modify microscopic intramolecular structures.(Fig.6) The average bond length of H-H and D-D is both more elongated (1) as the D_2 mixing ratio decreases, (2) as the temperature decreases, and (3) as the nonequilibrium flow forms. (Fig.6(a)) The solvation structures in the 2D

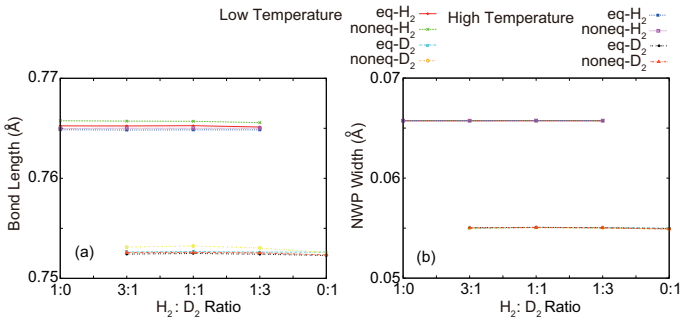

Fig. 6 (a) Average bond length and (b) average NWP width in the mixtures.

mixture films become denser in the situations (1)-(3), making the bonds attracted by the EWPs located at the bond center of neighboring solvating molecules.[31,33–38] We emphasize that the difference between the bond length of H-H and D-D purely originates from the different NQEs of hydrogen and deuterium nuclei such as more delocalized hydrogen NWPs and less delocalized deuterium NWPs; a traditional quantum chemistry calculation treating each nucleus as a point mass could not reproduce the different H-H and D-D bond length with the same thermodynamic condition. In fact, the NWP width directly links to the bond length (Fig.6(b)); the more elongated the bond length is, the more delocalized the NWPs are and *vice versa*. It is notable that the difference only in the atomic mass set as 1.00794 for H and 2.01410 for D in the NEWPMD method caused all the differences between the H_2 and D_2 molecules reported in this paper.

4 Conclusions

In summary, we for the first time calculated the purely isotopic mixtures composed of the H_2 and D_2 molecules rapidly flowing inside the nanoscale CNT. The NEWPMD method computationally disclosed that the originally more supercooled the mixture is in the equilibrium state, the more supercooled the mixture becomes in the nonequilibrium state due to the isotope-dependent flow-induced condensation. In any mixtures, the stronger supercooling of H_2 molecules than D_2 molecules in the equilibrium state becomes more enhanced under the nonequilibrium flow; the present effective molar volume is more cramped for the more delocalized H_2 molecules than for the less delocalized D_2 molecules–the differently pronounced NQEs of the purely isotopic molecules essentially influence the condensed adsorption and nonequilibrium flows taking place in the nanoscale CNT. Actually, the flow-induced condensed adsorption is almost absent for the D_2 molecules especially at the low temperature. The above insights for the condensed adsorption appearing in the nanoscale CNT under the nonequilibrium flow could not be obtained only by a single molecule-surface potential adsorption. It is one of the great advantages of the NEWPMD method that it can describe the various kinds of the locally condensed structures and thermodynamic phases including the nanoscale shear flow appearing in the 2D mixture films adsorbed around the CNT well. The possibility of the quantum sieving depending on the differently pronounced NQEs can be seen as the structural and dynamical difference along the z-direction especially appearing in Figs.2(g-i) and Fig.3(f). The isotope-dependent flow-induced condensation we found in this paper indicates that a condensed mixture of purely isotopic molecules, H_2 and D_2 molecules, possessing the same EWPs but the twice different mass can be effectively separated by a rapid nonequilibrium flow made inside a narrow nanoscale pore, opening a new strategy and innovative design of nanofluidic devices for the efficient kinetic quantum sieving of a condensed H_2-D_2 mixture not of a dilute gas mixture.

5 Author contributions

I.Y.C performed data curation, formal analysis, methodology, and visualization. S.Y. contributed to methodology. K.H.D. did conceptualization, investigation, methodology, supervision, and writing.

6 Conflict of interest

The authors declare no competing financial interest.

7 Acknowledgment

KHD thanks Kusunoki 125, PRESTO, Japan Science and Technology Agency Grant No.22713147, Grant-in-Aids for Scientific Research from Japan Society for the Promotion of Science (KAKENHI) Grant Nos. 20K05419 and 18H05407, and Toyota Mobility Foundation.

References

1 P. C. Souers, *Hydrogen Properties for Fusion Energy*, University of California Press, Berkeley, USA, 1986.

2 M. Kuhnel, J. M. Fernandez, F. Tramonto, G. Tejeda, E. Moreno, A. Kalinin, M. Nava, D. E. Galli, S. Montero and R. E. Grisenti, *Phys. Rev. B*, 2014, **89**, 180201.

3 D. Colognesi, U. Bafile, M. Celli, M. Neumann and A. Orecchini, *Phys. Rev. E*, 2015, **92**, 012311.

4 B. J. Kozioziemski and G. W. Collins, *Phys. Rev. B*, 2003, **67**, 174101.

5 D. White and J. R. Gaines, *J. Chem. Phys.*, 1965, **42**, 4152–4158.
6 M. Zoppi, M. Celli and A. K. Soper, *Phys. Rev. B*, 1998, **58**, 11905–11910.
7 G. Galliero and C. Boned, *Phys. Rev. E*, 2009, **80**, 061202.
8 M. Ceriotti, J. More and D. E. Manolopoulos, *Comp. Phys. Commun.*, 2014, **185**, 1019–1026.
9 F. Uhl, D. Marx and M. Ceriotti, *J. Chem. Phys.*, 2016, **145**, 054101.
10 G. Han, Y. Gong, H. Huang, D. Cao, X. Chen, D. Liu and C. Zhong, *ACS Appl. Mater. Interfaces*, 2018, **10**, 32128–32132.
11 J. Duan, J. Bai, B. Zheng, Y. Li and W. Ren, *Chem. Commun.*, 2011, **47**, 2556–2558.
12 H. Lyu, Q. Zhang, Y. Wang and J. Duan, *Dalton Trans.*, 2018, **47**, 4424–4427.
13 N. Behera, J. Duan, W. Jin and S. Kitagawa, *EnergyChem*, 2021, **3**, 100067.
14 Q. Wang, S. R. Challa, D. S. Sholl and J. K. Johnson, *Phys. Rev. Lett.*, 1999, **82**, 956–959.
15 J. Teufel, H. Oh, M. Hirscher, M. Wahiduzzaman, L. Zhechkov, A. Kuc, T. Heine, D. Denysenko and D. Volkmer, *Adv. Mater.*, 2013, **25**, 635–639.
16 H. Oh, I. Savchenko, A. Mavrandonakis, T. Heine and M. Hirscher, *ACS Nano*, 2014, **8**, 761–770.
17 B. Chen, X. Zhao, A. Putkham, K. Hong, E. B. Lobkovsky, E. J. Hurtado, A. J. Fletcher and K. M. Thomas, *J. Am. Chem. Soc.*, 2008, **130**, 6411–6423.
18 H. Kagita, T. Ohba, T. Fujimori, H. Tanaka, K. Hata, S.-I. Taira, H. Kanoh, D. Minami, Y. Hattori, T. Itoh, H. Masu, M. Endo and K. Kaneko, *J. Phys. Chem. C*, 2012, **116**, 20918–20922.
19 B. A. Danilchenko, I. I. Yaskovets, I. Y. Uvarova, A. V. Dobin, V. B. Eselson, R. M. Basnukaeva and N. A. Vinnikov, *Appl. Phys. Lett.*, 2014, **104**, 173109.
20 A. V. Dolbin, V. B. Eselson, V. G. Gavrilko, V. G. Manzhelii, N. A. Vinnikov, R. M. Basnukaeva, I. I. Yaskovets, I. Y. Uvarova and B. A. Danilchenko, *Low Temp. Phys.*, 2014, **40**, 246–250.
21 C. I. Contescu, H. Zhang, R. J. Olsen, E. Mamontov, J. R. Morris and N. C. Gallego, *Phys. Rev. Lett.*, 2013, **110**, 236102.
22 Y. Xing, J. Cai, L. Li, M. Yang and X. Zhao, *Phys. Chem. Chem. Phys.*, 2014, **16**, 15800–15805.
23 S. Yamaoka and K. Hyeon-Deuk, *J. Phys. Chem. Lett.*, 2022, **13**, 3579–3585.
24 M. Majumder, N. Chopra, R. Andrews and B. J. Hinds, *Nature*, 2005, **438**, 44–44.
25 J. K. Holt, H. G. Park, Y. Wang, M. Stadermann, A. B. Artyukhin, C. P. Grigoropoulos, A. Noy and O. Bakajin, *Science*, 2006, **312**, 1034–1037.
26 L. Fu, S. Merabia and L. Joly, *J. Phys. Chem. Lett.*, 2018, **9**, 2086–2092.
27 M. Nazari, A. Davoodabadi, D. Huang, T. Luo and H. Ghasemi, *ACS Nano*, 2020, **14**, 16348–16391.
28 M. Whitby and N. Quirke, *Nat. Nanotechnol.*, 2007, **2**, 87–94.
29 M. A. Gallis, J. R. Torczynski, D. J. Rader, M. Tij and A. Santos, *Phys. Fluids*, 2006, **18**, 017104.
30 B. Xu and X. Chen, *Phys. Chem. Chem. Phys.*, 2013, **15**, 1164–1168.
31 K. Hyeon-Deuk and K. Ando, *Phys. Rev. B*, 2014, **90**, 165132.
32 K. Hyeon-Deuk and K. Ando, *J. Chem. Phys.(Communication)*, 2014, **140**, 171101.
33 K. Hyeon-Deuk and K. Ando, *Phys. Chem. Chem. Phys.*, 2016, **18**, 2314–2318.
34 K. Hyeon-Deuk and K. Ando, *J. Chem. Phys.(Communication)*, 2015, **140**, 171102.
35 K. Abe and K. Hyeon-Deuk, *J. Phys. Chem. Lett.*, 2017, **8**, 3595–3600.
36 K. Abe, S. Yamaoka and K. Hyeon-Deuk, *J. Phys. Chem. B*, 2018, **122**, 8233–8242.
37 S. Yamaoka and K. Hyeon-Deuk, *J. Phys. Chem. Lett.*, 2020, **11**, 4186–4192.
38 S. Yamaoka and K. Hyeon-Deuk, *Phys. Chem. Chem. Phys.*, 2021, **23**, 22110–22118.
39 K. Hyeon-Deuk and K. Ando, *Chem. Phys. Lett.*, 2012, **532**, 124–130.
40 S. Grimme, J. Antony, S. Ehrlich and H. Krieg, *J. Chem. Phys.*, 2010, **132**, 154104.
41 N. Faginas-Lago, D. Yeni, F. Huarte, Y. Wang, M. Alcami and F. Martin, *J. Phys. Chem. A,*, 2016, **120**, 6451–6458.
42 G. Kresse and J. Furthmüller, *Phys. Rev. B*, 1996, **54**, 11169–11186.
43 J. A. Thomas and A. J. H. McGaughey, *Nano Lett.*, 2008, **8**, 2788–2793.
44 A. Noy, H. G. Park, F. Fornasiero, J. K. Holt, C. P. Grigoropoulos and O. Bakajin, *Nano Today*, 2007, **2**, 22–29.
45 G. Hummer, J. Rasaiah and J. Noworyta, *Nature*, 2001, **414**, 188–190.
46 X. Qin, Q. Yuan, Y. Zhao, S. Xie and Z. Liu, *Nano Lett.*, 2011, **11**, 2173–2177.
47 A. Berezhkovskii and G. Hummer, *Phys. Rev. Lett.*, 2002, **89**, 064503.
48 M. Khademi and M. Sahimi, *J. Chem. Phys.*, 2011, **135**, 204509.
49 J. Su and H. Guo, *J. Chem. Phys.*, 2011, **134**, 244513.
50 B. Paschke, D. Denysenko, B. Bredenkötter, G. Sastre, A. Wixforth and D. Volkmer, *Chem. Eur. J.*, 2019, **25**,

10803–10807.

Electronic Supplementary Information for "Anomalously Supercooled H_2-D_2 Mixtures Flowing inside a Carbon Nano Tube"

I-Ya Chang, Shutaro Yamaoka, and Kim Hyeon-Deuk*

Department of Chemistry, Kyoto University, Kyoto, 606-8502, Japan

E-mail: kim@kuchem.kyoto-u.ac.jp,Phone:+81-75-753-4021

*To whom correspondence should be addressed

S1: COMPUTATIONAL DETAILS

All the density functional theory (DFT) calculations were done with the PBE functional and PAW pseudopotentials implemented in the VASP package.[1] The length of the periodic unit cell is 8.52 Å along the CNT(15,0) axis (z-axis) while the vacuum of approximately 1 nm and 2 nm was inserted into the x- and y-directions, respectively. The energy cutoff for the plane wave basis is 400 eV. The Grimme D2 correction (PBE-D2) was employed and the scaling parameter s_6 in the PBE-D2 scheme was set as 0.6 with the other parameters remained as default values.[2] The validity of the current PBE-D2 setting was well-confirmed in the reproduction of the H_2-benzene interaction energy calculated by the accurate post Hartree-Fock methods, that is, the MP2/aug-ccpVQZ method and the CCSD(T)/complete basis set method.[2] We calculated the total energy of a diatomic molecule and CNT(15,0), $E_{tot}(R, \chi_{CNT})$, by the PBE-D2 scheme as a two dimensional (2D) function of the distance R and the angle $\chi_{CNT} = 0, \pi/12, \pi/6, \pi/4, \pi/3, 5\pi/12$, and $\pi/2$ graphically defined in Fig.S3. The analytical function of the total energy,

$$E_{tot}(R, \chi_{CNT}) = a\left[\left(\frac{b(\chi_{CNT})}{R}\right)^{6.8} - \left(\frac{b(\chi_{CNT})}{R}\right)^{5.5}\right], \tag{1}$$

was obtained by fitting the DFT-calculated total energy data points with the two coefficients a and $b(\chi_{CNT})$. While the coefficient $a = 8255.74$ K was found to be almost independent of χ_{CNT}, the other coefficient $b(\chi_{CNT})$ was obtained as a function of χ_{CNT} (Fig.S3(c)):

$$b(\chi_{CNT}) = 1.558 + \exp\left[-\frac{\cos^2\chi_{CNT}}{10.6}\right] \simeq 2.558 - \frac{\cos^2\chi_{CNT}}{11.1}. \tag{2}$$

The interaction potential energy between the molecule and CNT(15,0), $E_{CNT}(R)$ shown in Fig.S4, was calculated further by symmetrically averaging $E_{tot}(R, \chi_{CNT})$ with respect to

χ_{CNT} to take into account the symmetric interaction of the molecule with CNT(15,0):

$$E_{CNT}(R) = \frac{1}{4\pi}\int_0^{\pi} \sin\chi_{\mathrm{CNT}} d\chi_{CNT} \int_0^{2\pi} d\omega_{CNT} E_{tot}(R, \chi_{\mathrm{CNT}}). \quad (3)$$

The molecule-CNT(15,0) interaction force $\mathbf{F}_{CNT}$ equally acting on two nuclei composing the same molecule was calculated from the gradient of $E_{CNT}(R)/2$, and added to eq.(1).

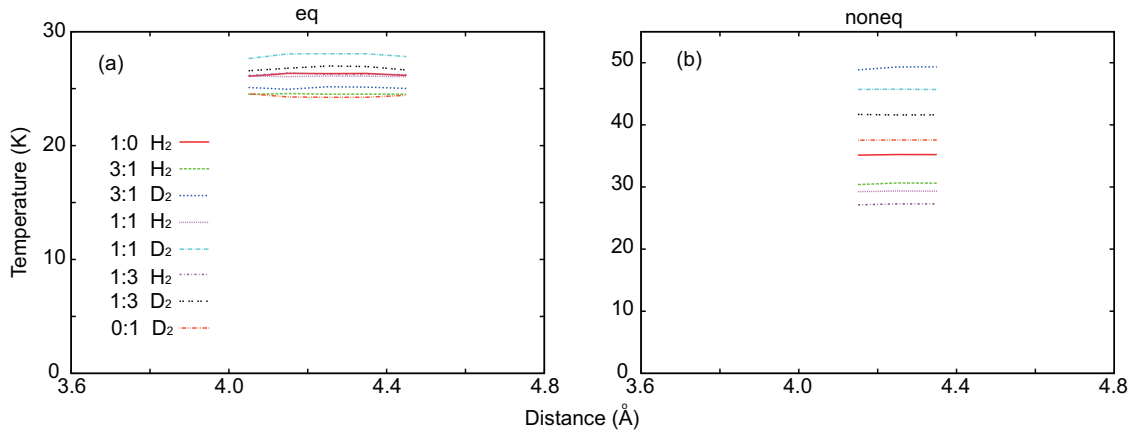

Figure S1: Temperature as a function of the radial distance whose origin is located at the CNT(15,0) center in (a) the equilibrium states at the high temperature and (b) the nonequilibrium states at the high temperature. No data is shown in the region where the molecules can hardly visit during the current 3 ns simulations. In all the cases, the temperature is almost uniform and higher in the nonequilibrium states than in the equilibrium states. The order of the average temperature in the nonequilibrium states is determined by the extent of the flow velocity (Fig.S9(f)) as well as the molecular mass order: On one hand, the faster the nonequilibrium flow is, the higher the average temperature is. On the other hand, the heavier the mixture mass is, the higher the average temperature is. The totally lower temperatures of the H_2 molecules achieved in the nonequilibrium states contribute to the stronger supercooling of the H_2 molecules.

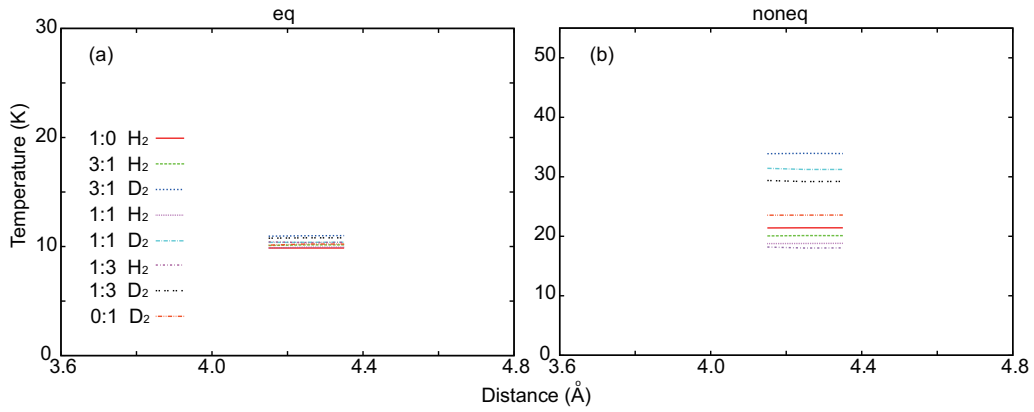

Figure S2: The same as Fig.S1 but at the low temperature. The order of the average temperature in the nonequilibrium states is also determined by the extent of the flow velocity (Fig.S10(f)) as well as the molecular mass order. The totally lower temperatures of the H_2 molecules achieved in the nonequilibrium states contribute to the stronger supercooling of the H_2 molecules.

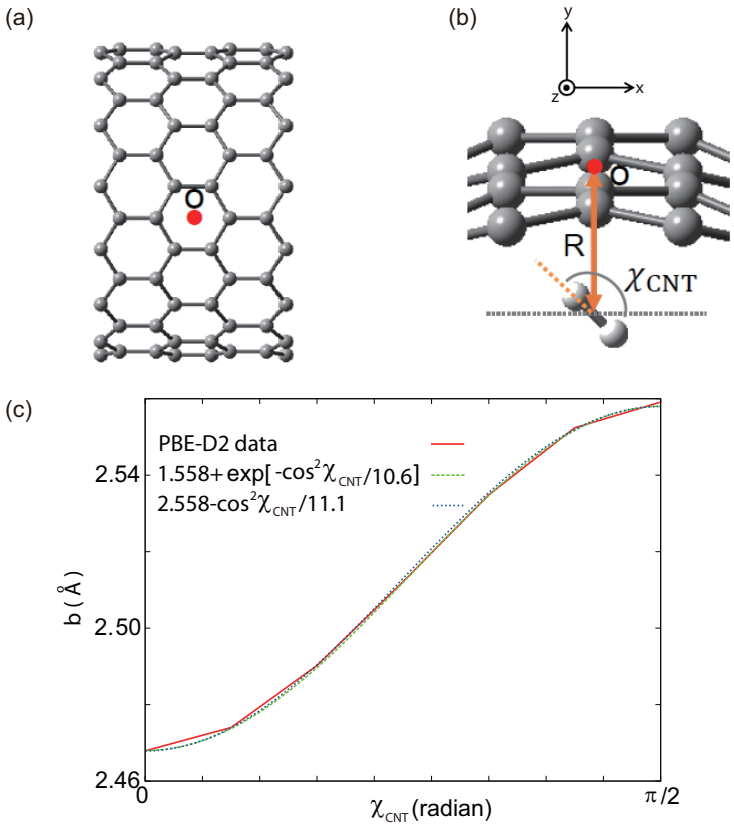

Figure S3: (a) Adsorption site **o** on the CNT(15,0) surface located at the center of a carbon ring of CNT(15,0). (b) Distance R between the center of mass (COM) of a diatomic molecule and the adsorption site **o**. χ_{CNT} is an angle between the molecular axis and the x-axis. (c) Coefficient $b(\chi_{CNT})$ as a function of χ_{CNT}.

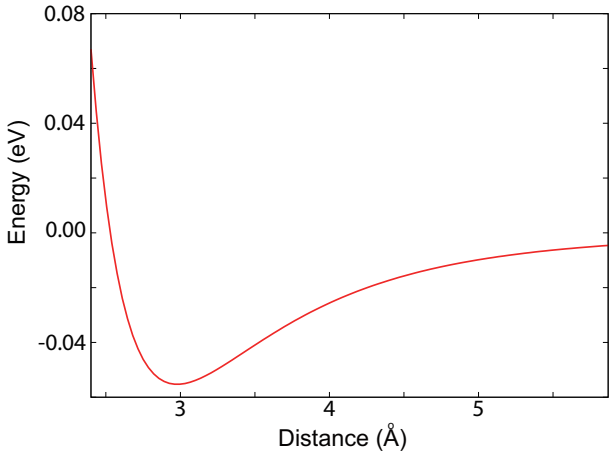

Figure S4: Interaction potential energy between the molecule and CNT(15,0), $E_{CNT}(R)$, as a function of the distance R defined in Fig.S3(b).

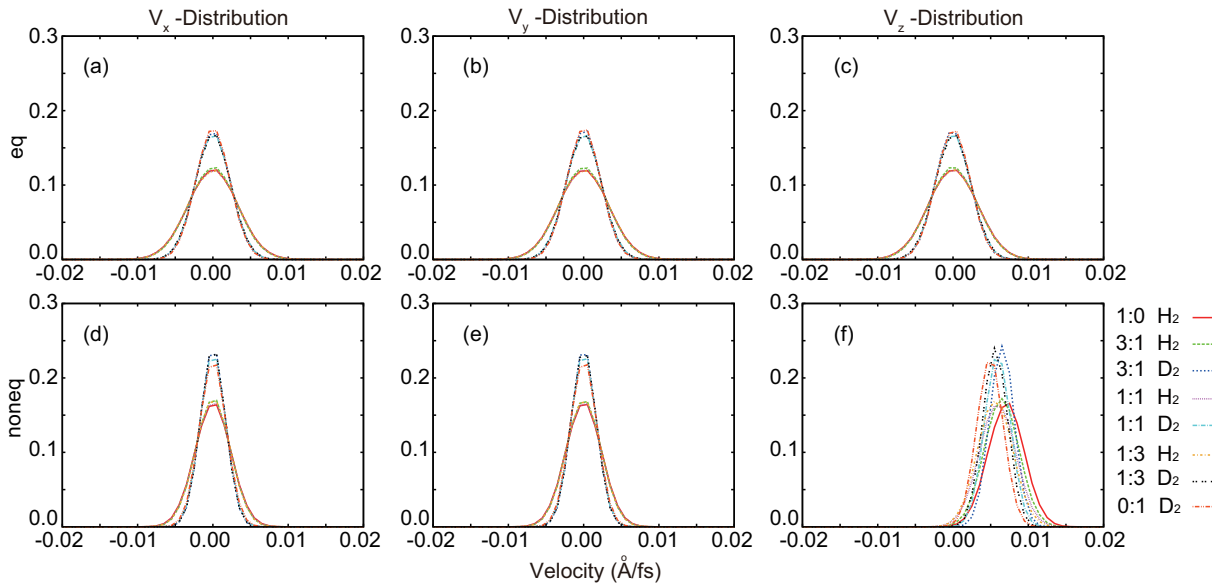

Figure S5: Distributions of the COM velocity V_x, V_y, and V_z at the high temperature (a-c) in the equilibrium states and (d-f) under the nonequilibrium flows. The distributions are broader for the lighter H_2 molecules than for the heavier D_2 molecules. The peak V_z velocity is the same regardless of the isotopes in the same mixture, being in harmony with Figs.S9 and S10. The nonequilibrium flow makes the **V**-distributions sharper due to the flow-induced condensation. The average values of V_x, V_y, and V_z are shown in Fig.S9.

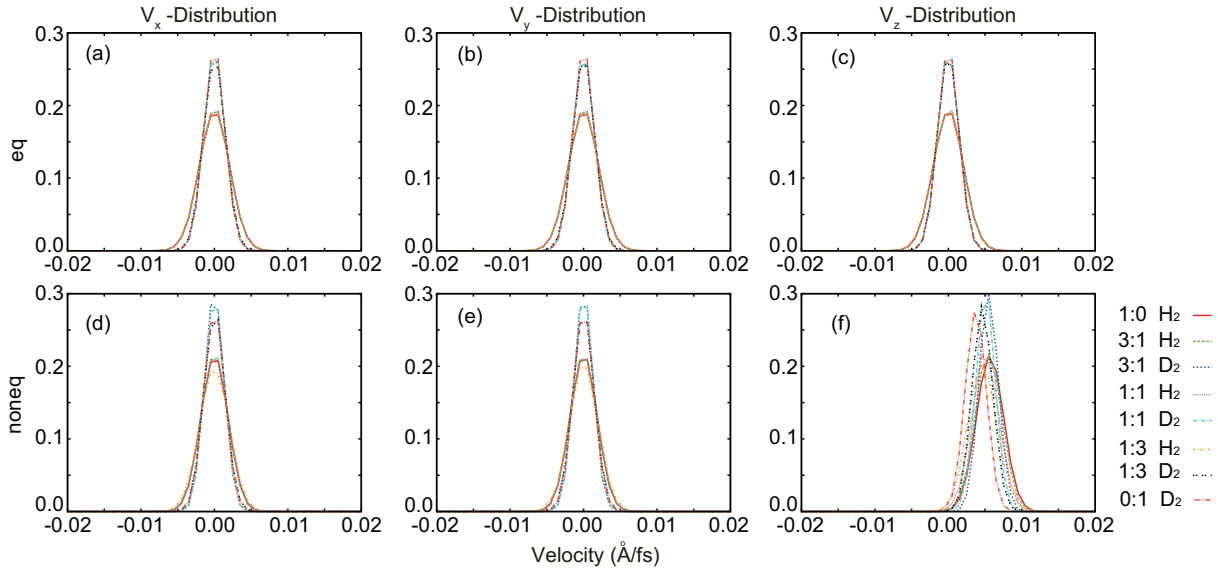

Figure S6: The same as Fig.S5 but at the low temperature. All the distributions become sharper at the low temperature than at the high temperature regardless of the mixing ratios both in the equilibrium and nonequilibrium states. The average values of V_x, V_y, and V_z are shown in Fig.S10.

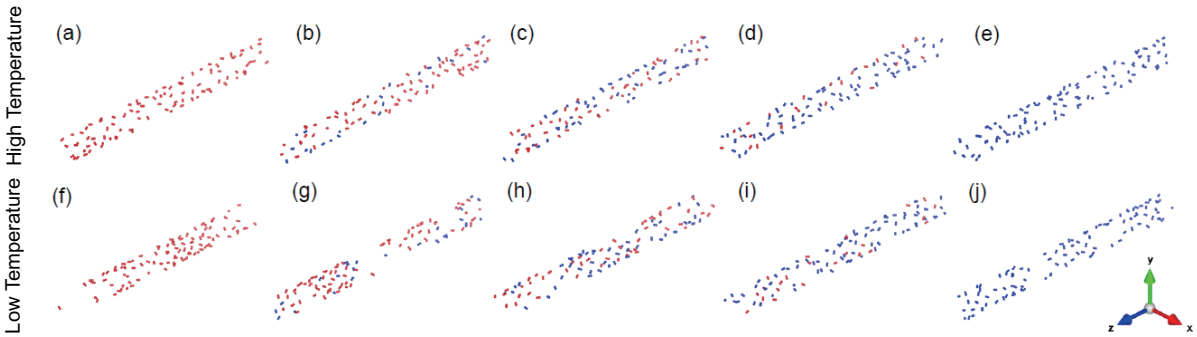

Figure S7: Snapshots of the H_2 (red) and D_2 (blue) molecules at (a-e) the high temperature and (f-j) the low temperature confined inside CNT(15,0) in the equilibrium states. The D_2 ratio increases as (a,f) 0 %, (b,g) 25 %, (c,h) 50 %, (d,i) 75 %, and (e,j) 100 % from the left to the right. The confined 2D mixture films become clearly more structured and non-uniform at the low temperature.

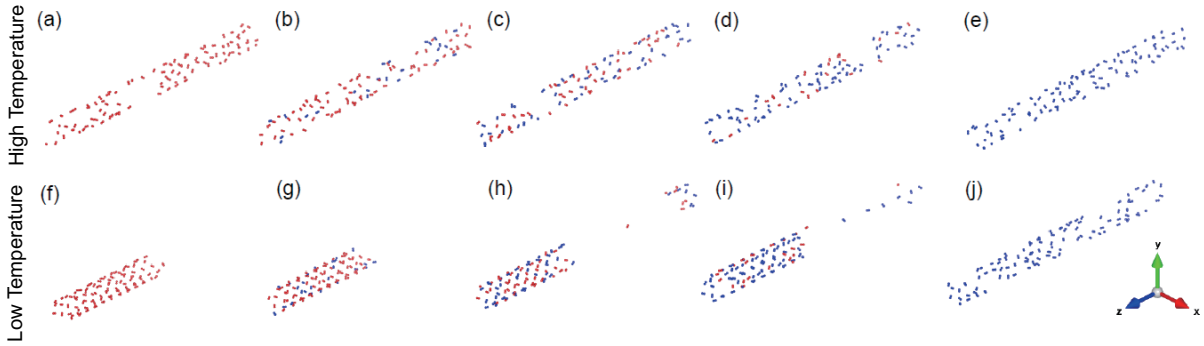

Figure S8: The same as Fig.S7 but under the nonequilibrium flow. In the nonequilibrium state, the structures of the 2D mixture films become non-uniform even at the high temperature.

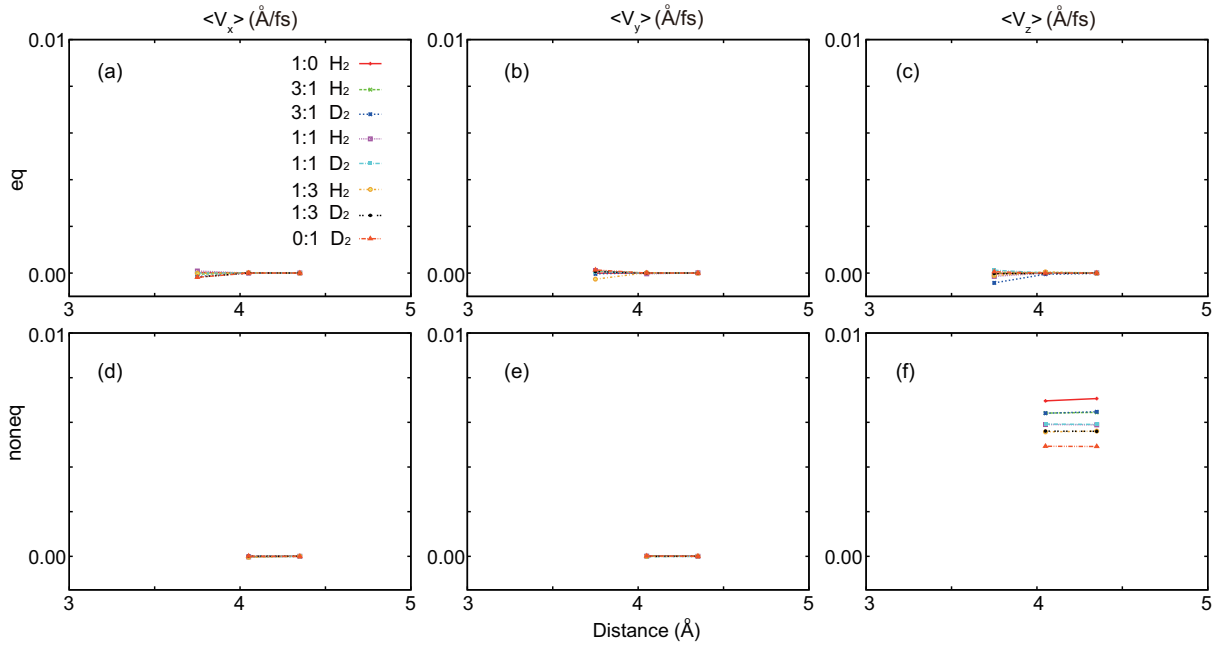

Figure S9: Average velocity as a function of the radial distance from the CNT(15,0) center, $\langle V_x \rangle$, $\langle V_y \rangle$, and $\langle V_z \rangle$ at the high temperature (a-c) in the equilibrium states and (d-f) under the nonequilibrium flows. No data is shown in the region where any molecules can rarely visit during the 3 ns simulations. $\langle V_x \rangle$ and $\langle V_y \rangle$ are almost zero regardless of the mixing ratio both in the equilibrium and nonequilibrium states. $\langle V_z \rangle$ in the equilibrium states is also almost zero. $\langle V_z \rangle$ has a slight gradient along the radial distance under the nonequilibrium flow, meaning that a nonequilibrium shear flow exists inside CNT(15,0). The overall values of $\langle V_z \rangle$ are smaller as the D_2 mixing ratio becomes higher since the heavier liquids are harder to accelerate. Note that $\langle V_z \rangle$ of the H_2 and D_2 molecules are almost identical in the same mixture because of the energy exchange among all the molecules through the intermolecular interaction.

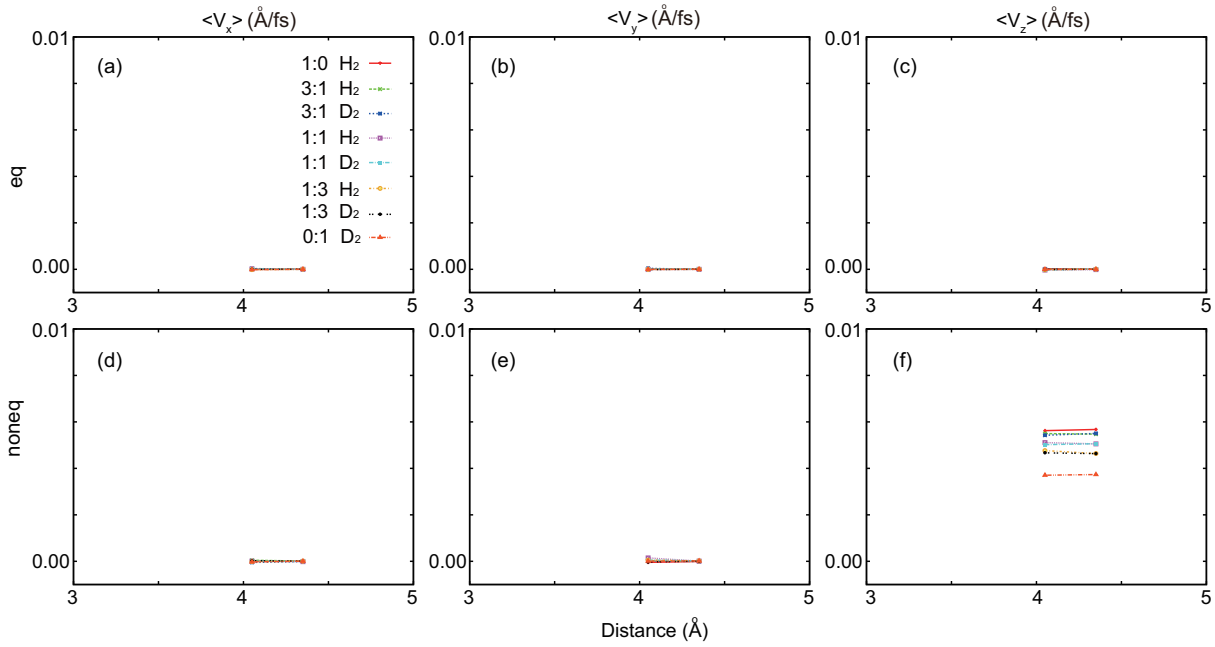

Figure S10: The same as Fig.S9 but at the low temperature.

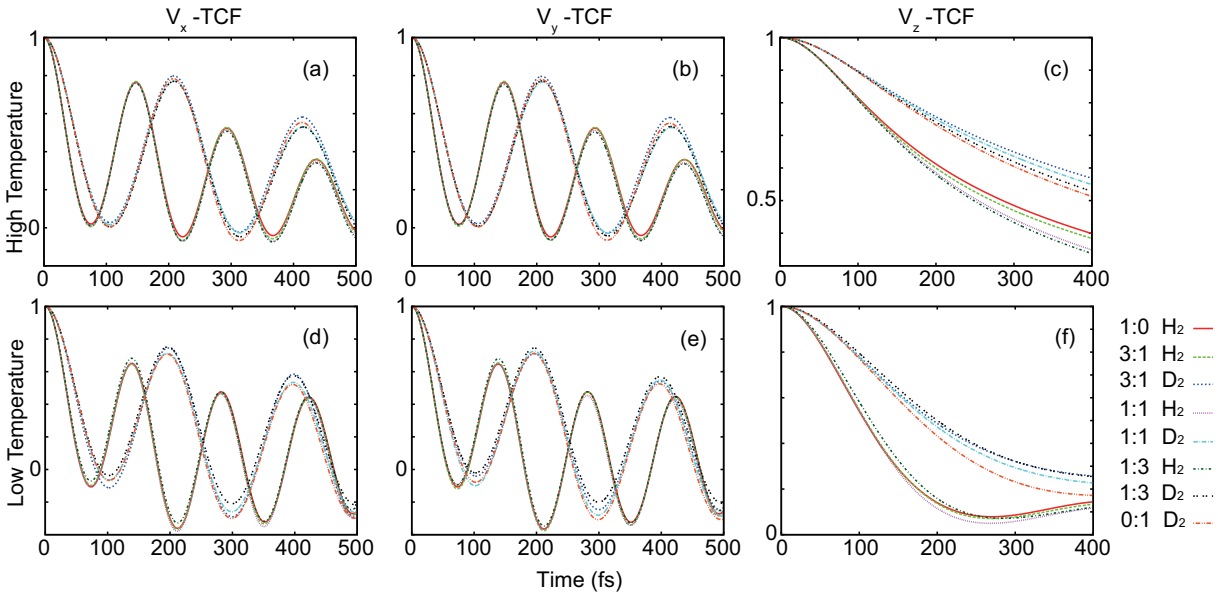

Figure S11: The same as Fig.3 but in the equilibrium states.

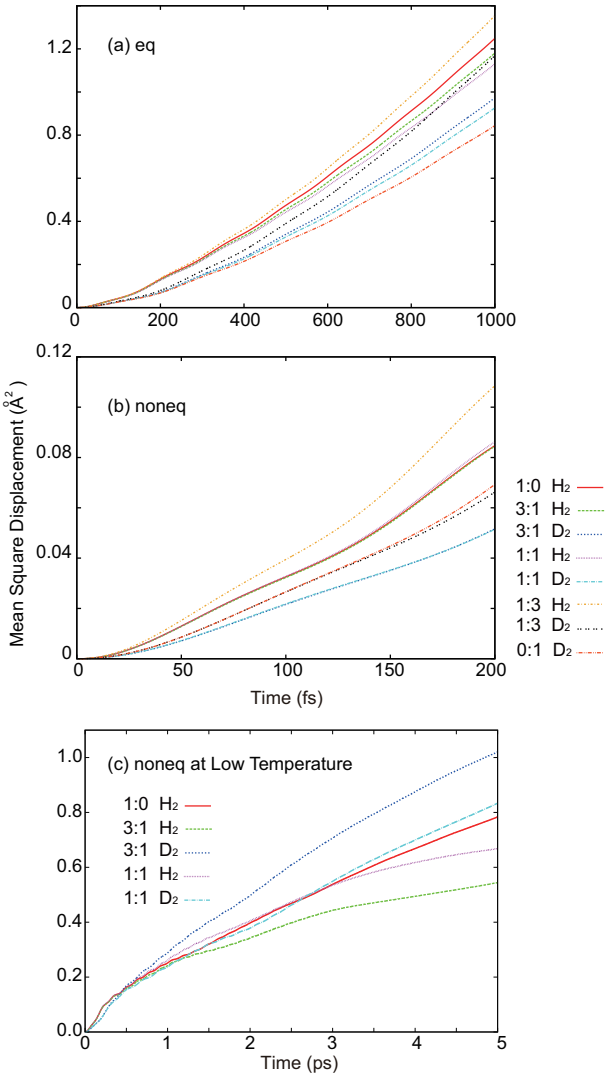

Figure S12: Initial mean-square-displacements at the low temperature in the (a) equilibrium and (b) nonequilibrium states. (c) Magnified Fig.4(d) without the 1:3 and 0:1 mixtures.

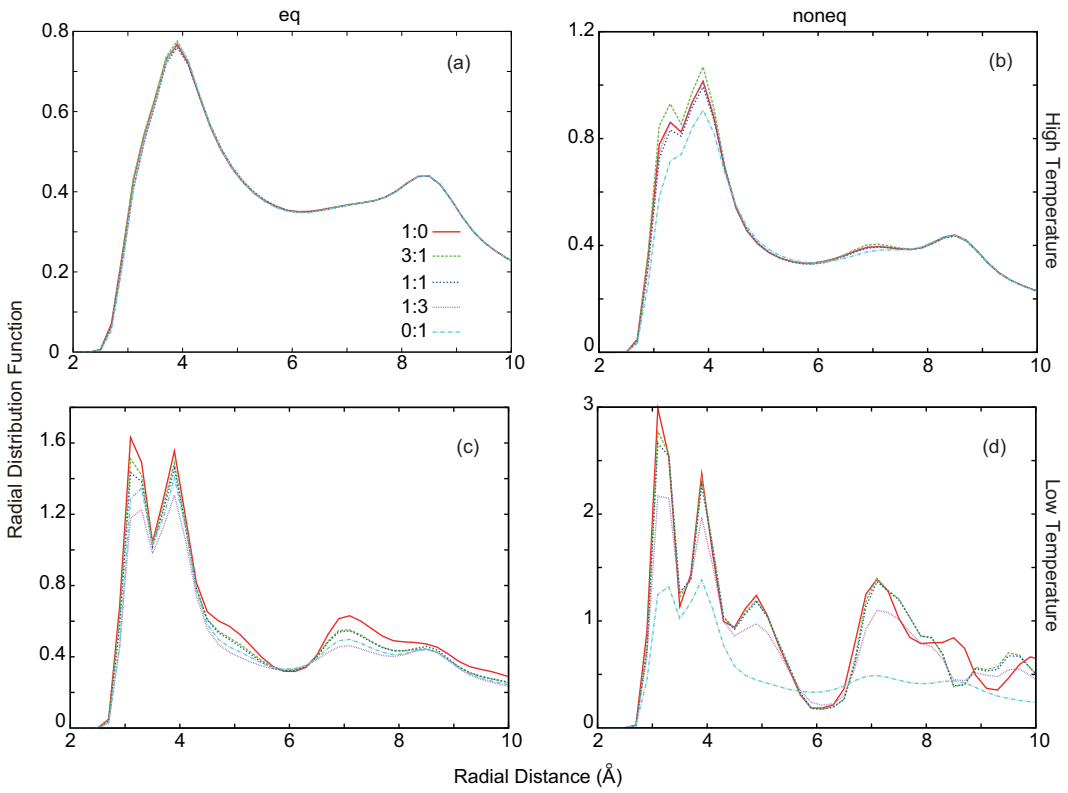

Figure S13: Radial distribution functions (RDFs) at (a) the high temperature in the equilibrium states, (b) the high temperature under the nonequilibrium flows, (c) the low temperature in the equilibrium states, and (d) the low temperature under the nonequilibrium flows. Because the 0:1 mixture exhibits little flow-induced condensation at the low temperature as shown in Fig.1(j), the RDFs are almost similar in the equilibrium and nonequilibrium states, resulting in the smallest RDF of the 0:1 mixture under the nonequilibrium flow.(The light-blue line in Fig.S13(d))

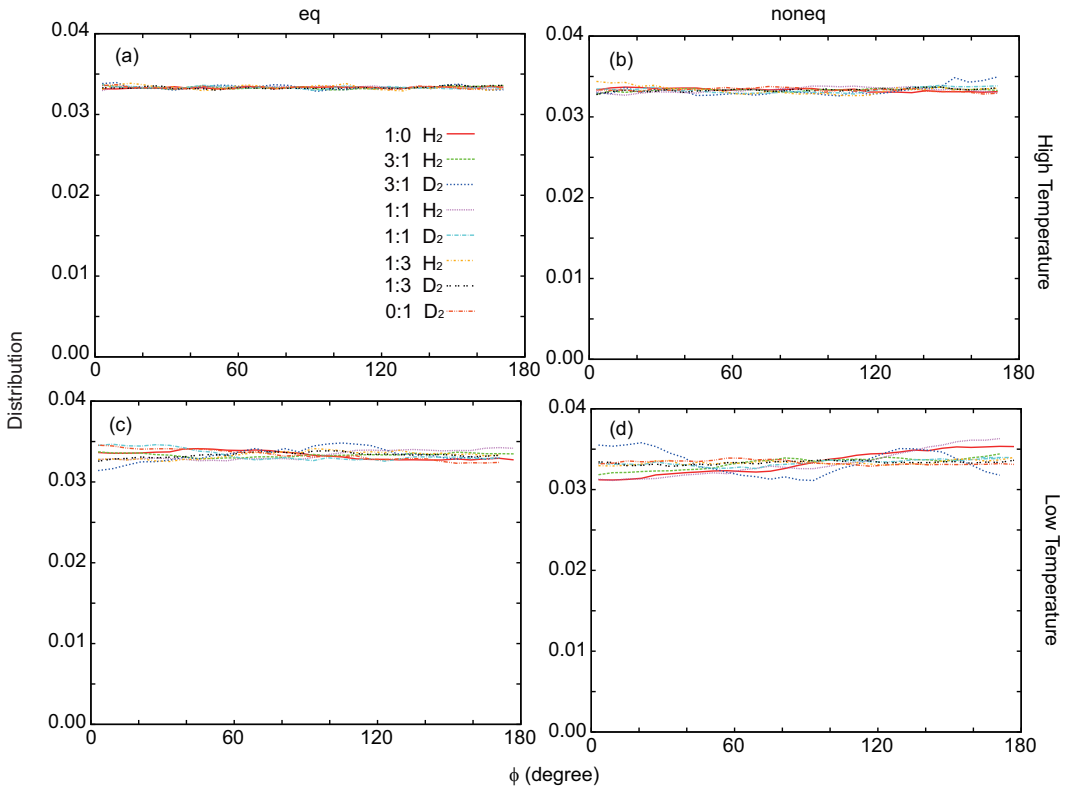

Figure S14: Distributions of the molecular orientation $\phi(t)$ from the z-axis at (a) the high temperature in the equilibrium states, (b) the high temperature under the nonequilibrium flows, (c) the low temperature in the equilibrium states, and (d) the low temperature under the nonequilibrium flows. The ϕ-distributions are almost uniform regardless of the mixing ratio and thermodynamic conditions.

References

(1) Kresse, G.; Furthmüller, J. *Phys. Rev. B* **1996**, *54*, 11169–11186.

(2) Faginas-Lago, N.; Yeni, D.; Huarte, F.; Wang, Y.; Alcami, M.; Martin, F. *J. Phys. Chem. A,* **2016**, *120*, 6451–6458.